Regular Article

# Dissociative ionization of the potential focused electron beam induced deposition precursor $\pi$ -allyl ruthenium(II) tricarbonyl bromide, a combined theoretical and experimental study\*<sup>†</sup>

Maicol Cipriani<sup>1</sup>, Rachel M. Thorman<sup>2</sup>, Christopher R. Brewer<sup>3</sup>, Lisa McElwee-White<sup>3</sup>, and Oddur Ingólfsson<sup>1,a</sup>

- <sup>1</sup> Science Institute and Department of Chemistry, University of Iceland, Dunhagi 3, 107 Reykjavík, Iceland
- <sup>2</sup> Department of Chemistry, Johns Hopkins University, Baltimore, USA
- <sup>3</sup> Department of Chemistry, University of Florida, Gainesville, FL 32611-7200, USA

Received 18 March 2019 / Received in final form 26 July 2019 Published online 29 October 2019

 $\odot$ EDP Sciences / Società Italiana di Fisica / Springer-Verlag GmbH Germany, part of Springer Nature, 2019

**Abstract.** Here we present a combined theoretical and experimental study on dissociative ionization of  $(\eta^3$ -allyl)Ru(CO)<sub>3</sub>Br, a potential precursor for focused electron beam induced deposition. Experimental appearance energies are determined by electron impact ionization and relative cross sections for selected fragmentation channels are presented from their respective thresholds to about 70 eV incident electron energy. Threshold energies for individual fragmentation channels are computed at the hybrid density functional and coupled cluster level of theory and compared to the respective experimental appearance energies.

### 1 Introduction

Focused electron beam induced deposition (FEBID) is a nanofabrication technique with the capability of directly writing three-dimensional nanostructures by metal deposition on uneven surfaces with a tightly focused, highenergy electron beam [1–3]. Deposition is the result of electron induced reactions causing fragmentation of the precursor molecules, which are continuously supplied to the substrate surface. Ideally, FEBID precursors should dissociate completely upon interaction with the high-energy electron beam, creating pure deposits of well-defined composition confined to the area exposed to the electron beam. However, the interaction of a high-energy primary electron beam with a substrate produces backscattered and secondary electrons with a broad energy distribution. The energy distribution of the secondary electrons produced in this process generally ranges from close to 0 eV to about 100 eV, peaks below 10 eV and has a substantial value at energies close to 0 eV [4,5]. These low-energy secondary electrons may be significantly more plentiful at the point of interaction on the substrate surface than the high-energy primary electrons [1,6] and may cause fragmentation of the

precursor molecules [7–11]. Further, the low-energy electron induced fragmentation processes may have considerable cross sections (see e.g. Refs. [11,12] and references therein). Such low-energy electron induced fragmentation typically results in incomplete decomposition and ligand co-deposition, and is thus relevant to deposit purity. In fact, currently used FEBID precursors commonly lead to low purity deposits and deposits broadening beyond the dimension of the primary beam [1,2]. This is mainly due to the spatial distribution of the backscattered and thus low-energy secondary electrons. Generally, low-energy electrons can induce fragmentation through four distinct processes, as shown in equations (1)–(4): Dissociative Ionization (DI, (1)), Dissociative Electron Attachment (DEA, (2)), Neutral Dissociation (ND, (3)) and Dipolar Dissociation (DD, (4)).

$$AB + e^{-} \rightarrow AB^{\#+} + 2e^{-} \rightarrow A^{\#+} + B^{\#} + 2e^{-}$$
 (1)

$$AB + e^- \to AB^{\#-} \to A^{\#-} + B^{\#}$$
 (2)

$$AB + e^{-}(\epsilon_1) \to [AB]^* + e^{-}(\epsilon_2 < \epsilon_1) \to A^{\#} + B^{\#}$$
 (3)

$$AB + e^{-}(\epsilon_1) \to [AB]^* + e^{-}(\epsilon_2 < \epsilon_1) \to A^{\#+} + B^{\#-}.$$
 (4)

Here the hash, #, indicates that the transient negative ion (TNI) and/or the fragments produced may be in an electronically and/or vibrationally excited state, while the asterisk, \*, indicates an electronic excitation. In support of the efforts to develop high performance FEBID precursors, it is important to understand the energy dependence and the extent of these electron-induced processes

<sup>\*</sup> Contribution to the Topical Issue "Dynamics of Systems on the Nanoscale (2018)", edited by Ilko Bald, Ilia A. Solov'yov, Nigel J. Mason and Andrey V. Solov'yov.

<sup>†</sup>Supplementary material in the form of one pdf file available from the Journal web page at https://doi.org/10.1140/epjd/e2019-100151-9.

<sup>&</sup>lt;sup>a</sup> e-mail: odduring@hi.is

with current and potential FEBID precursors, and to compare such data with their decomposition on surfaces and their actual performance under real FEBID conditions. In this context several studies on electron-induced decomposition of FEBID precursors in the gas phase under single collision conditions (see e.g. Refs. [11,13–16] and Refs. therein) and at surfaces under controlled UHV conditions have been conducted (see e.g. Refs. [17–19] and Refs. therein). The comparison of such gas phase and surface data has also been reported in collaborative studies (see e.g. Refs. [11,20]) and most recently this approach has been extended by comparing the gas phase decomposition of the bimetallic precursor HFeCo<sub>3</sub>(CO)<sub>12</sub> with its decomposition under electron exposure at surfaces under controlled UHV conditions and its deposition performance under actual high-vacuum FEBID conditions [21].

In this context we have studied dissociative electron attachment (DEA) to  $(\eta^3$ -allyl)Ru(CO)<sub>3</sub>Br in detail [22,23], using this potential precursor as a model compound with three different types of ligands with distinctly different properties. The same compound has also been studied with regards to its fragmentation and deposition properties when adsorbed on a substrate surface and exposed to 500 eV electrons under controlled UHV conditions [24]. Most recently FEBID and reductive post purification of  $\pi$ -allyl ruthenium(II) tricarbonyl has also been reported [25], showing 23 at. % content in the initial deposition and 83 at. % after treatment with 2% hydrogen in a nitrogen gas. However, in these experiments significant volume reduction was observed after the purification step. These studies are particularly interesting as FEBID has been developed on a commercial scale for photo mask repair, and due to its fairly high transparency in the extreme ultraviolet regime, ruthenium is commonly used as a capping layer in the currently emerging EUVL masks [26]. Current Ru precursors are limited, and the only ones we are aware of are  $Ru_3(CO)_{12}$  [27] and bis(ethylcyclopentadienyl) ruthenium(II) [26,28] thus providing an additional motivation for our current study of  $(\eta^3$ -allyl)Ru(CO)<sub>3</sub>Br. In the current contribution, we extend our previous studies on  $(\eta^3$ -allyl)Ru(CO)<sub>3</sub>Br by presenting the energy dependence of the relative cross sections for electron impact ionization and dissociative ionization of this potential FEBID precursor. Furthermore, we use the onset of the positive ion yield curves to estimate the ionization energy and appearance energies (AEs) for the principal dissociative ionization fragmentation channels. Further, threshold energies for the principal fragmentation channels, at the PBE0 [29,30] and DLPNO-CCSD(T) [31–33] level of theory are reported and compared to the respective experimental AEs.

### 2 Method

### 2.1 Quantum chemical calculations

All calculations were performed using ORCA [34]. All structures were optimized at the PBE0 (hybrid GGA functional) [29,30]/def2-TZVP [35] (using the def2 effective core potential [35] for the ruthenium core electrons), including the D3(BJ) dispersion correction by Grimme

et al. [36,37]. PBE0 and BP86 [38,39] (GGA functional) have both been found to give very reliable structures of transition metal complexes [40–42]. However, in thermochemical studies on transition metal compounds, PBE0 is often among the best performers [43–45]. Thus, for comparison PBE0 threshold values are reported along with the threshold values calculated at the coupled cluster level of theory. Also a comparison with threshold values calculated at the BP86 level of theory is given as Supplementary Material (Tab. SI1). Harmonic vibrational frequencies were calculated at the PBE0/def2-TZVP level of theory. They were confirmed to be positive and were used to derive zero point vibrational energy and thermal energy corrections. Potential alternate isomers and spin states were investigated in order to make sure that the lowest energy state was indeed determined for each fragment. Coupled cluster calculations were performed on optimized geometries at the DLPNO-CCSD(T) [31–33] level of theory, using DZ/TZ extrapolation (def2-SVP [35] and def2-TZVP), auxiliary def2-QZVPP/C [46] basis set and ECPs: def2-ECP (for Ru). Quasi-restricted orbitals [47] were used as a reference in the coupled cluster calculations, which reduces spin contamination from the UHF step.

### 2.2 Experimental

Positive ion yield curves and mass spectra were recorded with an electron-molecule crossed beam setup that has been previously described in detail [48]. Only a brief description is given here. The crossed beam setup consists of a trochoidal electron monochromator (TEM), an effusive gas inlet and a commercial quadrupole mass spectrometer (QMS) (Hiden EPIC1000, Hiden Analytical, Warrington UK). The quasi mono-energetic electron beam is crossed with the effusive target gas, generated by sublimation of solid  $(\eta^3$ -allyl)Ru(CO)<sub>3</sub>Br at room temperature, entering the reaction region through a capillary tube. The typical background pressure was around  $4 \times 10^{-8}$  mbar and experiments were carried out with a target gas pressure in the range from 3 to  $6 \times 10^{-7}$  mbar in order to assure single collision conditions. The gas temperature is assumed to be that of the inlet system (room temperature), but the monochromator was heated to 120°C with two halogen lamps in order to avoid deposition of the target compound on the electrical lens components. The electron energy was calibrated using the  $SF_6$  formation from  $SF_6$  at  $0\,\mathrm{eV}$  electron energy and the energy resolution was estimated from the full width at half maximum of that signal and was found to be in the range from 120–140 meV in the current study. Mass spectra were recorded at fixed electron impact energy, typically 70–75 eV, by scanning through the relevant m/z range and ion yield curves were recorded at fixed m/z ratios by scanning through the relevant electron energy range. The ions formed in the crossed beam region were extracted by a small electric field (typically <1 V/cm) and focused onto the entrance aperture of the quadrupole mass spectrometer. The extraction time from the point of origin to the entrance of the QMS was in the range of  $20-30\,\mu s$ , depending on the voltage setting and the mass of the respective ions. To allow better

Table 1. Experimentally determined ionization and AEs for the principal fragments observed in electron impact ionization and fragmentation of  $(\eta^3$ -allyl)Ru(CO)<sub>3</sub>Br compared to the respective threshold values calculated at the PBE0/ def2-TZVP and at the DLPNO-CCSD(T) Extrapolate(2/3,def2) def2-TZVP/C level of theory (including ZPE and thermal energy of the neutral molecules).

Fragment	m/z	AE	PBE0 / def2-TZVP	DLPNO-CCSD(T) Extrapolate(2/3, def2) def2-QZVPP/C
$[(\pi - C_3H_5)Ru(CO)_3Br]^+$	306	$8.6 \pm 0.6 (\pm 0.6)$	7.99	8.20
$[(\pi-C_3H_5)Ru(CO)_2Br]^+$	278	$9.9 \pm 0.5 (\pm 0.1)$	9.43	9.57
$[(\pi - C_3H_5)Ru(CO)Br]^+$	250	$10.8 \pm 0.5 (\pm 0.2)$	10.76	10.58
$[(\pi-C_3H_5)RuBr]^+$	222	$13.3 \pm 0.5 (\pm 0.5)$	12.77	12.34
$[Ru(CO)_3Br]^+$	265	$12.9 \pm 0.6 (\pm 0.6)$	10.13	10.40
$[Ru(CO)_2Br]^+$	237	$13.4 \pm 0.5 (\pm 0.5)$	12.24	12.29
[Ru(CO)Br] <sup>+</sup>	209	$15.7 \pm 0.5(\pm 0.5)$	15.31	15.59
[RuBr] <sup>+</sup>	181	$16.6 \pm 0.6 (\pm 0.6)$	17.65	17.02
$[(\pi - C_3 H_5) Ru]^+$	143	$15.9 \pm 0.5 (\pm 0.1)$	15.15	14.33
[RuC] <sup>+</sup>	114	$17.4 \pm 0.5(\pm 0.4)$	$21.96^{\star}(18.6^{\star\star})$	20.44*(17.11**)
[Ru]+	102	$18.8 \pm 0.5 (\pm 0.5)$	18.74	17.81

<sup>\*</sup>Assuming that the carbon originates from the allyl group and that H<sub>2</sub> is formed in the fragmentation process (see Eq. (7))

comparison between the relative cross sections for individual fragmentation channels, the respective ion yields were normalized to the pressure, and the  ${\rm Ar}^+$  ion yield from Ar at 70 eV incident electron energy recorded for each specific experiment:

$$I_{\text{Norm.}} = \left(\frac{I_{m/z}}{I_{Ar_{r_0, \text{eV}}^+}}\right) \left(\frac{p_{Ar}}{p_{Ru}}\right).$$
 (5)

Here  $I_{m/z}$  is the spectral intensity of a particular m/z fragment from the  $(\eta^3$ -allyl)Ru(CO)<sub>3</sub>Br and  $p_{Ru}$  is the partial pressure of  $(\eta^3$ -allyl)Ru(CO)<sub>3</sub>Br during a particular measurement.  $I_{Ar_{70\,\mathrm{eV}}^+}$  and  $p_{Ar}$  are the measured  $Ar^+$  ion yields at 70 eV and the Ar pressure during the same measurement, respectively.

For determination of the appearance energies, the energy scale was recalibrated using the AE of Ar<sup>+</sup> with Ar as the target gas [49]. The onset of the ion yields were fitted with a Wannier type function [50] of the form:

$$E \le AE, f(x) = b$$
  

$$E > AE, f(x) = b + a(E - AE)^{d}.$$
(6)

Here, E represents the energy of the incident electron, AE represents the appearance energy, b is a constant that considers the background signal, a is a scaling coefficient, and d is an exponential factor. Examples of these fits can be found in the ESI. The resulting ion yield curves for each fragment were obtained with the average of multiple scans recorded after each other. The fitting error from fitting equation (6) to these data sets ranges from <0.1 eV to about 0.6 eV. We, however, estimate the confidence limit to rather be in the range of 0.5 eV, as only one data set is behind each fit. These are the confidence limits reported, but in Table 1 and Table SI1 the fitting errors are also reported in parenthesis. The  $(\eta^3$ -allyl)Ru(CO)<sub>3</sub>Br was synthesized as previously reported [51], purified by sublimation at 30°C and 90 mTorr and characterized by comparison with literature values [51,52].

### 3 Results and discussion

Figure 1 shows a positive ion mass spectrum resulting from electron impact ionization and dissociation of  $(\eta^3$ -allyl)Ru(CO)<sub>3</sub>Br at 75 eV incident electron energy. The mass spectrum is characterized by three progressions: i) loss of 1-3 CO ligands, ii) loss of the allyl group and 0-3 CO ligands, and iii) the loss of bromine and 0-3 CO ligands. The most prominent of these progressions is that of the loss of 1-3 CO ligands and interestingly, most of the intensity in the other two progressions is in the m/z ratios reflecting the loss of all three CO units along with the loss of the allyl group and bromine, respectively. In addition to these three regressions, RuCO<sup>+</sup>, RuC<sup>+</sup> and Ru<sup>+</sup> are observed with fair intensities. Figure 2 shows the respective positive ion yield curves for (a) the loss of 1-3 CO units and (b) the loss of the allyl group and 0-3 CO units. Such progressions of CO loss are commonly observed in dissociative ionization of carbonyl containing FEBID precursors. The formation of the bare metal ion with appreciable intensity is common in dissociative ionization of pure metal carbonyls, but is generally less efficient for other organometallic species (see for example Refs [53–55] and Refs therein). The ion yield in the energy range from 0-70 eV electron incident energy and an expansion of the threshold region is shown in the lower panels (c and d). For better comparison, the ion yield curve for the formation of the parent ion is shown in all panels and all ion yields are normalised with respect to pressure and the Ar<sup>+</sup> ion yield measured at 70 eV, see equation (5). The experimental AEs for these fragments, determined by fitting equation (6) to the threshold region, are shown in Table 1 along with the respective threshold values calculated at the PBE0/ def2-TZVP and at the DLPNO-CCSD(T) Extrapolate(2/3,def2) def2-QZVPP/C level of theory. Also shown are the calculated threshold values for the loss of bromine (or bromide), three CO units and for the formation of Ru<sup>+</sup>, RuC<sup>+</sup> and RuCO<sup>+</sup>. The experimental AEs and the calculated threshold values are

<sup>\*\*</sup> Assuming Br formation through dipolar dissociation, but otherwise as shown in equation (7).

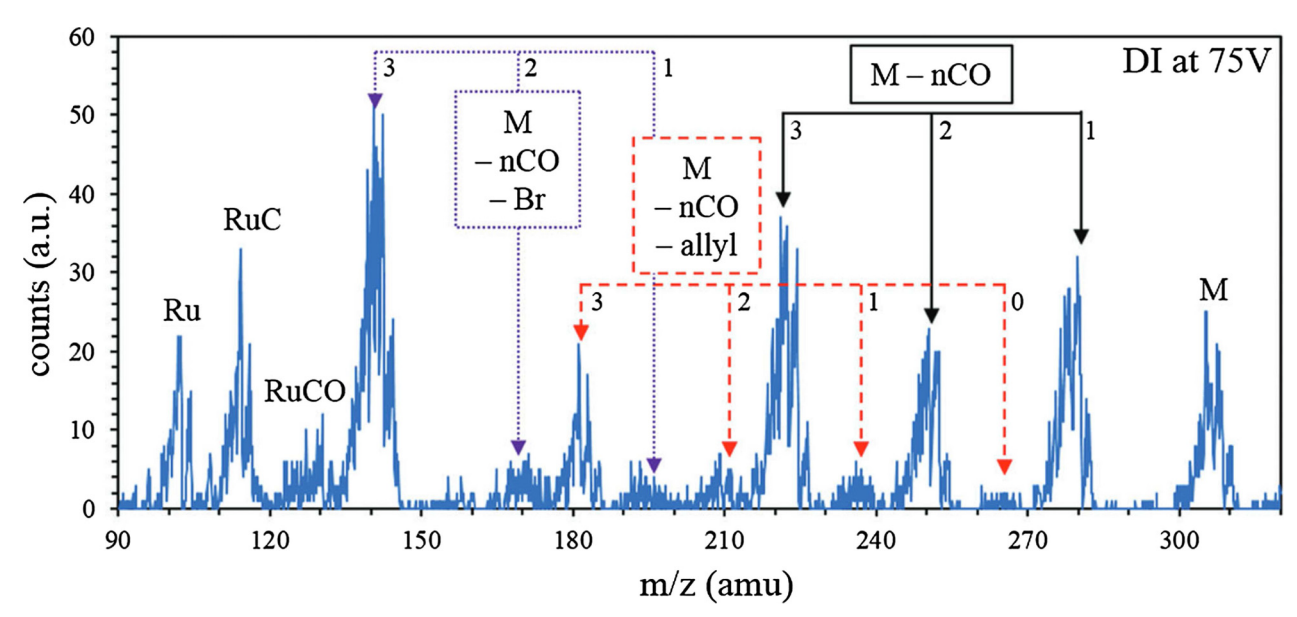


Fig. 1. Electron impact ionization mass spectrum of  $(\eta^3$ -allyl)Ru(CO)<sub>3</sub>Br recorded at 75 eV incident electron energy. The main channels observed are sequential carbonyl loss (1-3 CO), allyl loss accompanied by sequential carbonyl loss (0-3 CO), and bromine loss accompanied by sequential carbonyl loss (1-3 CO). Reproduced from reference [22] with permission from the PCCP Owner Societies.

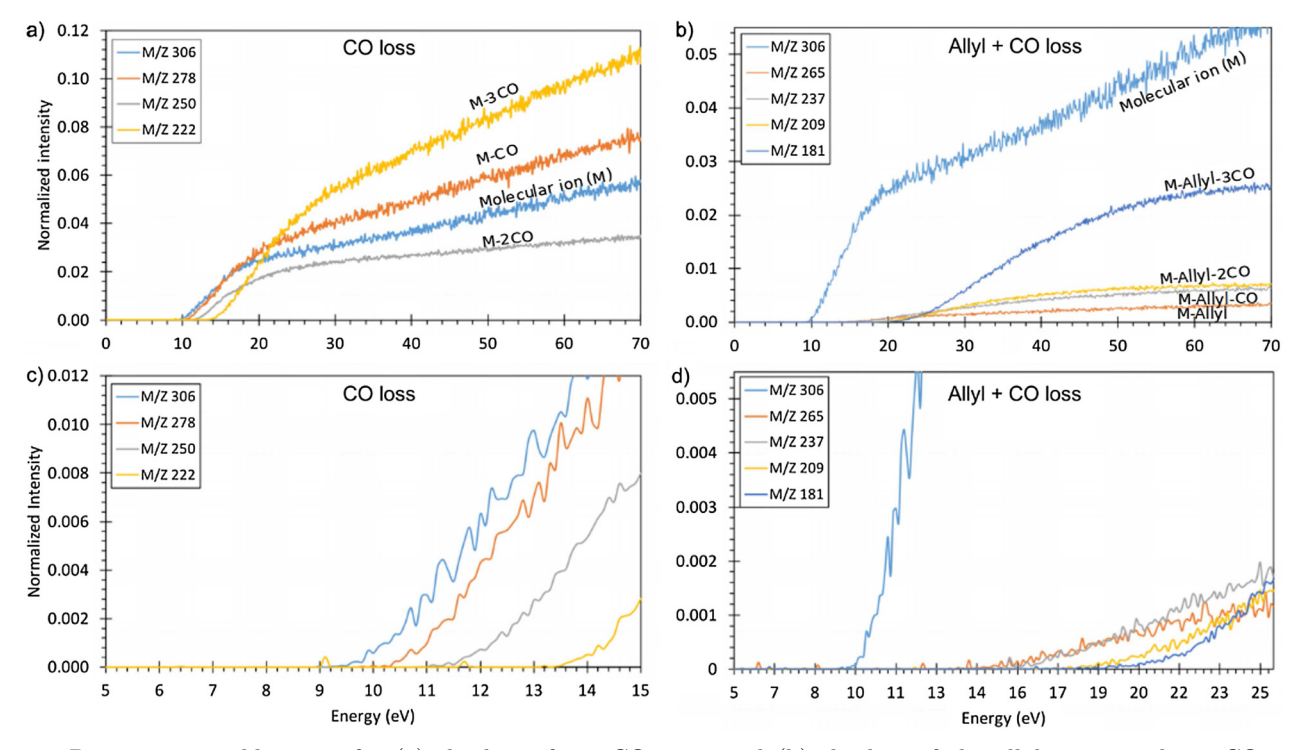


Fig. 2. Positive ion yield curves for (a) the loss of 1-3 CO units and (b) the loss of the allyl group and 0-3 CO units. The ion yield curves are shown in the incident electron energy range from below threshold to about  $70 \,\mathrm{eV}$  and an expansion of the threshold region is shown in the lower panels (c and d). All ion yields are normalised with respect to the pressure and the  $\mathrm{Ar}^+$  ion yield from Ar at  $70 \,\mathrm{eV}$  incident electron energy recorded for each specific experiment, see equation (5). For better comparison the ion yield curve for the formation of the parent ion is shown in all panels.

further compared in Figure 3, which also shows the optimized structures of the respective cationic fragments (the x,y,z files are provided with SI). Here, the AE for m/z 306 corresponds to the IE of  $(\eta^3$ -allyl)Ru(CO)<sub>3</sub>Br and is

experimentally determined to be  $8.6\,\mathrm{eV}$ . The adiabatic IE calculated at the DLPNO-CCSD(T) Extrapolate(2/3, def2) def2-QZVPP/C level of theory is  $8.20\,\mathrm{eV}$ . Considering the confidence limits of the experimental values, the

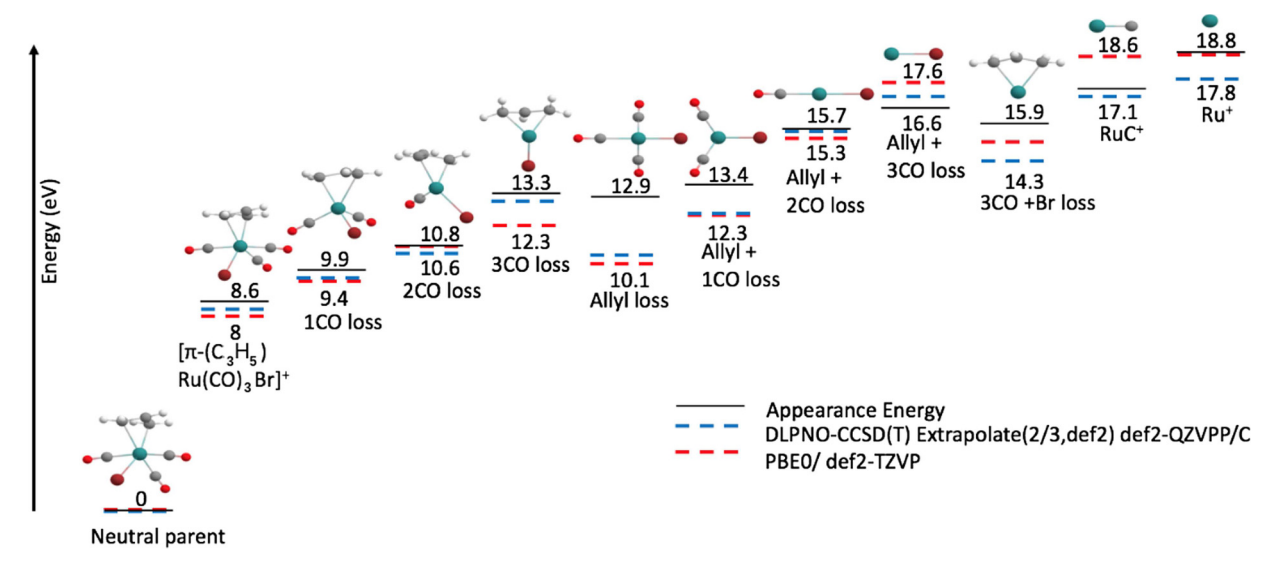


Fig. 3. Optimized structures and threshold energies for charged fragments observed in dissociative ionization of  $(\eta^3$ -allyl)Ru(CO)<sub>3</sub>Br. Also shown are the experimentally determined AEs for the respective fragments. The structural optimization was carried out at the PBE0/def2-TZVP level of theory and the threshold energies were calculated at the PBE0/def2-TZVP and at the DLPNO-CCSD(T) Extrapolate(2/3,def2) def2-TZVP/C levels of theory. The optimized structure of the neutral molecule is shown as the origin (0 eV) of the energy axis. All numbers are in eV.

agreement is fairly good. The same is true for the threshold values for sequential CO loss, except for the coupled cluster value for the loss of 3 CO units, which is about 1 eV below the experimentally determined AE. The calculated values for the allyl loss and the allyl loss and one CO loss. on the other hand, are considerably lower than the experimental AEs for the loss of the allyl and the allyl and one CO unit. The calculated threshold value for the allyl loss and the loss of two CO units, on the other hand agrees comparably well with the experimentally determined AE. Turning back to the mass spectra shown in Figure 1 and the ion yield curves shown in Figure 2 it is clear that most of the intensity in this regression is from the loss of the allyl group and all three CO units. This may be due to a considerable kinetic shift in the allyl loss channel, making the allyl loss too slow to be observed at threshold in the current experimental setup. We note that this must be a substantial effect, as the observation window in the current setup is about 20–30  $\mu$ sec and the calculated threshold values are about 2.5 eV below the experimental AE for the allyl loss. However, presuming that all observed dissociation channels are from the cationic ground state, the allyl loss would compete with the energetically much more favourable, and presumably faster CO loss. This is further supported by the fact that the  $(\eta^3$ -allyl) group is a polyhapto ligand with a  $\pi$ -facial interaction of all three allyl carbons with the central Ru atom. Another possible explanation is that the initial allyl loss proceeds from an electronically excited cationic state that is considerably higher in energy than the ground state. In both of these cases, the excess energy is readily available for further CO loss after the initial allyl loss, which provides a rationale for the bulk of the intensity for this regression representing loss of the allyl group and all three CO units. Hence, reflecting the resilience of the allyl group and the lability of the CO units toward dissociation from the complex.

The remaining fragments, m/z 130, 114 and 102, are assigned to RuCO<sup>+</sup>, ruthenium carbide RuC<sup>+</sup> and Ru<sup>+</sup>, respectively. For RuC<sup>+</sup> we find the AE to be  $17.4\pm0.4\,\mathrm{eV}$  and the calculated threshold value, assuming that the carbon originates from the allyl group and that H<sub>2</sub> is formed in the process, is  $20.44\,\mathrm{eV}$ ;

$$(\eta^{3} - \text{allyl})\text{Ru(CO)}_{3}\text{Br} + \text{e}^{-} \rightarrow$$

$$[\text{RuC}]^{+} + \text{Br} + 3\text{CO} + \text{CH}_{2}\text{CH} + \text{H}_{2} + 2\text{e}^{-}.$$
(7)

However, presuming that this fragment results from dipolar dissociation leading to bromide formation, the threshold calculated at the coupled cluster level is found to be 17.11 eV, which is in good agreement with the experimental value. Previously we have reported gas phase DEA studies to  $(\eta^3$ -allyl)Ru(CO)<sub>3</sub>Br [22,23], and recently Spencer et al. [24] reported a study on the electron-induced decomposition of this compound when adsorbed on surfaces at low temperature under controlled UHV conditions. In the surface study by Spencer et al. [24], attention was given to comparison of the different ligands in the context of their suitability as leaving groups in FEBID precursors. The authors found that the electron-induced fragmentation of  $(\eta^3$ -allyl)Ru(CO)<sub>3</sub>Br adsorbed on surfaces, is characterized by an initial CO loss. Judging from the intensity in the O (1s) signal in their XPS spectra, about 80% of the CO is lost already after an irradiation of about  $4 \times 10^{16} \,\mathrm{e^-\,cm^{-2}}$ . Further electron irradiation of about  $5 \times 10^{18} \,\mathrm{e^-\,cm^{-2}}$  effectuated removal of the bulk of the bromine, but the carbon from the allyl group remained on the surface. Under gas phase single collision conditions, we find the most significant electron induced dissociation channel to be the loss of a single CO. In fact, the loss of CO ligands per incident electron in DI is about 2, while the CO loss per DEA incident is about 1 [22]. Further, other channels than

CO loss are insignificant in DEA, while both allyl and bromine loss is observed in DI of  $(\eta^3$ -allyl)Ru(CO)<sub>3</sub>Br in the gas phase. Thus neither the ligand loss as observed in DI in the gas phase under single collision conditions, nor that observed in DEA reflects the observations when  $(\eta^3$ -allyl)Ru(CO)<sub>3</sub>Br is adsorbed on surfaces and is exposed to 500 eV electrons [24]. Interestingly, in a very recent FEBID study [25] on  $\pi$ -allyl ruthenium(II) tricarbonyl bromide at room temperature, a reduction of the C:Ru ratio from the initial 6:1 found in the precursor to 2:1 in the deposit is observed; i.e., an average of 4 carbon atoms are lost during the deposition process. The O:Ru ratio in the deposit is similarly reduced to 0.3:1 from the initial 3:1. The authors interpret these observations as due to essentially complete CO loss, but also a partial allyl loss. They point out that the reason for the lack of allyl loss in the surface experiments may be due to the low temperature these are conducted at  $(-168^{\circ}\text{C})$ . No bromine loss is observed in the FEBID experiments, which is readily understandable as the FEBID experiments are conducted under quasi steady state conditions and bromine loss is only observed in the surface experiment after prolonged irradiation of the static monolayers initially deposited. In principle both DEA and DI may be active and one would expect their efficiency to reflect the energy dependence of their relative cross sections, convoluted with the energy distribution of the secondary electrons (see e.g. Ref. [11]). However, no desorption of bromine or the allyl group is observed from the initial fragmentation of  $(\eta^3$ -allyl)Ru(CO)<sub>3</sub>Br, when adsorbed on surfaces, and no bromine loss is observed in the FEBID experiments. This may in part be due to alteration of the dissociation efficiency when  $(\eta^3$ -allyl) Ru(CO)<sub>3</sub>Br is adsorbed on surfaces and/or be the result of hindered desorption of ligands through ligand-surface interaction or the compounds orientation on the surface. Furthermore, the surface may offer an efficient heat bath for vibrational cooling, quenching the presumably slower allyl loss more efficiently than the CO loss. Such ligand stabilization has been observed for clusters in general [56], but more relevant for the current study, this effect has also been observed in clusters of the FEBID precursor Fe(CO)<sub>5</sub> [57]. We also note that no information on ND is provided here and this may also be a very effective channel, as has been shown in the case of  $Pt(PF_3)_4$  [58].

## 4 Conclusion

In the current contribution we have determined threshold energies for positive ion formation from  $(\eta^3\text{-allyl})\text{Ru}$  (CO)<sub>3</sub> Br, computed at the PBE0/def2-TZVP and DLPNO -CCSD(T) Extrapolate(2/3,def2) def2-QZVPP/C level of theory. These were compared to the respective experimental IE and AEs estimated from the onsets of the respective electron impact ion yield curves. The computed structure of the molecular cation and the respective fragments, optimized at the PBE0/def2-TZVP level of theory, were also presented as well as the experimentally acquired ion yields for sequential CO loss and the loss of the allyl group and 1-3 CO ligands. The presented data

were discussed in the context of previous DEA studies on  $(\eta^3$ -allyl)Ru(CO)<sub>3</sub>Br [22,23], and in the context of a study on electron-induced decomposition of this precursor adsorbed on surfaces at low temperature under controlled UHV conditions [24], and in context to a very recent FEBID study on this compound [25]. Dissociative ionization of  $(\eta^3$ -allyl)Ru (CO)<sub>3</sub>Br is characterized by three progressions: sequential loss of the CO ligands, loss of the allyl group and 0-3 CO ligands and loss of the bromine and 0-3 CO ligands. Among these, the sequential CO loss has the highest integral intensity, but the loss of the allyl group and the bromine along with 3 CO units is also significant. Further fragments observed in DI of  $(\eta^3$ -allyl)Ru(CO)<sub>3</sub>Br are the bare ruthenium cation Ru<sup>+</sup>, the ruthenium carbide cation RuC<sup>+</sup>, and RuCO<sup>+</sup>. In general, the coupled cluster calculations agree better with the experimental results than the calculations using the PBE0 functional. The agreement with the experimental AEs for sequential CO loss is fairly good, considering the confidence limits on the experimental data. However, the AE for the allyl loss alone is more than 2.5 eV above the calculated values. The difference is smaller (1.0 eV) for the loss of the allyl group along with three additional CO ligands and is only 0.4 eV for the loss of the allyl group and two CO ligands (calculated at the coupled cluster level of theory). We tentatively attribute this effect to delayed dissociation of the allyl group due to the trihapto nature of the  $\eta^3$ -allyl-ruthenium bond. This effect is strengthened through competition with the singly coordinated, presumably faster, direct CO loss channels. As has been discussed previously, DI of  $(\eta^3$ -allyl)Ru(CO)<sub>3</sub>Br leads to considerably more extensive fragmentation than DEA [22], and in contrast to DEA, DI leads to both significant allyl and bromide loss. In the previous surface study [24] the initial electron induced decomposition of  $(\eta^3$ -allyl)Ru(CO)<sub>3</sub>Br was found to be characterized by CO loss. Bromine loss was only observed in a second step after prolonged irradiation while loss of the allyl group was not observed. In the recent FEBID study [25] loss of all three CO ligands was observed as well as partial allyl loss, but no bromine loss was observed. The extent of the ligand loss in these experiments does not match directly with DEA or DI of this compound in the gas phase under single collision conditions, demonstrating the additional complexity introduced through surface interaction and eventual desorption barriers. Nonetheless similar to the observations in the surface experiments, CO loss is the dominating channel in both DI and DEA in the gas phase and much more efficient than the allyl loss. This further supports the assertion that polyhapto ligands are not suitable in FEBID precursors.

This work has been supported by the Icelandic Center of Research (RANNIS), Grant No. 13049305(1-3) and the University of Iceland Research Fund. M.C. acknowledges a doctoral grant from The Doctoral Grants of The University of Iceland Research Fund. It was conducted within the framework of the COST Action CM1301: Chemistry for ELectron-Induced Nano- fabrication (CELINA). RMT acknowledges financial support from the COST Action CM1301: CELINA for a short term scientific mission (STSM). L.M.-W. and C.R.B. thank the US National Science Foundation (Grant CHE- 1607547) for partial support of this work.

# References

- I. Utke, P. Hoffmann, J. Melngailis, J. Vac. Sci. Technol. B 26, 1197 (2008)
- W.F. van Dorp, C.W. Hagen, J. Appl. Phys. 104, 081301 (2008)
- M. Huth, F. Porrati, C. Schwalb, M. Winhold, R. Sachser, M. Dukic, J. Adams, G. Fantner, Beilstein J. Nanotechnol. 3, 597 (2012)
- 4. J. Schaefer, J. Hoelzl, Thin Solid Films 13, 81 (1972)
- 5. A.P. Knights, P.G. Coleman, Appl. Surf. Sci. 85, 43 (1995)
- N. Silvis-Cividjian, C.W. Hagen, H.A. Leunissen, P. Kruit, Microelectron. Eng. 61-62, 693 (2002)
- S. Engmann, M. Stano, Š. Matejčík, O. Ingólfsson, Phys. Chem. Chem. Phys. 14, 14611 (2012)
- S. Engmann, M. Stano, P. Papp, M.J. Brunger, Š. Matejčík, O. Ingólfsson, J. Chem. Phys. 138, 044305 (2013)
- O. May, D. Kubala, M. Allan, Phys. Chem. Chem. Phys. 14, 2979 (2012)
- K. Wnorowski, M. Stano, C. Matias, S. Denifl, W. Barszczewska, Š. Matejčík, Rapid Commun. Mass Spectrom. 26, 2093 (2012)
- R.M. Thorman, R.K. T.P., D.H. Fairbrother,
   O. Ingólfsson, Beilstein J. Nanotechnol. 6, 1904 (2015)
- P.C. Hoyle, J.R.A. Cleaver, H. Ahmed, Appl. Phys. Lett. 64, 1448 (1994)
- R.K. T.P., S. Barth, R. Bjornsson, O. Ingólfsson, Eur. Phys. J. D 70, 163 (2016)
- R.M. Thorman, I. Unlu, K.R. Johnson, R. Bjornsson, L. McElwee-White, D.H. Fairbrother, O. Ingólfsson, Phys. Chem. Chem. Phys. 20, 8 (2018)
- J. Kopyra, P. Maciejewska, J. Maljković, Beilstein J. Nanotechnol. 8, 2257 (2017)
- M. Allan, M. Lacko, P. Papp, Š. Matejčík, M. Zlatar, I.I. Fabrikant, J. Kočišek, J. Fedor, Phys. Chem. Chem. Phys. 20, 11692 (2018)
- 17. J.A. Spencer, Y.C. Wu, L. McElwee-White, D.H. Fairbrother, J. Am. Chem. Soc. 138, 9172 (2016)
- 18. R.K. T.P., I. Unlu, S. Barth, O. Ingólfsson, D.H. Fairbrother, J. Phys. Chem. C **122** (2017)
- 19. W.G. Garden, H. Lu, J.A. Spencer, D.H. Fairbrother, L. McElwee-White, MRS Commun. 8, 343 (2018)
- I. Unlu, J.A. Spencer, K.R. Johnson, R.M. Thorman, O. Ingólfsson, L. McElwee-White, D.H. Fairbrother, Phys. Chem. Chem. Phys. 20, 7862 (2018)
- R.K. T.P., P. Weorich, L. Hanefeld, R. Bjornsson, H.R. Hrodmarsson, S. Barth, D.H. Fairbrother, M. Huth, O. Ingólfsson, Beilstein J. Nanotechnol. 9, 555 (2018)
- R.M. Thorman, J.A. Brannaka, L. McElwee-White, O. Ingólfsson, Phys. Chem. Chem. Phys. 19, 13264 (2017)
- R.M. Thorman, R. Bjornsson, O. Ingólfsson, Eur. Phys. J. D. 70, 164 (2016)
- J.A. Spencer, J. Brannaka, M. Barclay, L. McElwee-White,
   D.H. Fairbrother, J. Phys. Chem. C 119, 15349 (2015)
- J. Jurczyk, C.R. Brewer, O.M. Hawkins, M.N. Polyakov, C. Kapusta, L. McElwee-White, I. Utke, ACS Appl. Mater. Interfaces 11, 28164 (2019)

- J.H. Noh, M.G. Stanford, B.B. Lewis, J.D. Fowlkes, H. Plank, P.D. Rack, Appl. Phys. A 117, 1705 (2014)
- V. Scheuer, H. Koops, T. Tschudi, Microelectron. Eng. 5, 423 (1986)
- C.M. Gonzalez, W. Slingenbergh, R. Timilsina, J.-H. Noh, M.G. Stanford, B.B. Lewis, K.L. Klein, T. Liang, J.D. Fowlkes, P.D. Rack, Proc. SPIE 9048, 90480M (2014)
- J.P. Perdew, K. Burke, M. Ernzerhof, Phys. Rev. Lett. 77, 3865 (1996)
- 30. C. Adamo, V. Barone, J. Chem. Phys. 110, 6158 (1999)
- 31. C. Riplinger, F. Neese, J. Chem. Phys. 138, 034106 (2013)
- C. Riplinger, B. Sandhoefer, A. Hansen, F. Neese, J. Chem. Phys. 139, 134101 (2013)
- C. Riplinger, P. Pinski, U. Becker, E. Valeev, F. Neese, J Chem Phys. 144, 024109 (2016)
- 34. F. Neese, WIREs Comput. Mol. Sci. 2, 73 (2012)
- F. Weigend, R.Ahlrichs, Phys. Chem. Chem. Phys. 7, 3297 (2005)
- S. Grimme, J. Antony, S. Ehrlich, H. Krieg, J. Chem. Phys. 132, 154104 (2010)
- S. Grimme, S. Ehrlich, L. Goerigk, J. Comput. Chem. 32, 1456 (2011)
- 38. A.D. Becke, Phys. Rev. A 38, 3098 (1988)
- 39. J.P. Perdew, Phys. Rev. B 33, 8822 (1986)
- M. Bühl, H. Kabrede, J. Chem. Theory Comput. 2, 1282 (2006)
- 41. M.P. Waller, H.Braun, N. Hojdis, M.Bühl, J. Chem. Theory Comput. 3, 2234 (2007)
- M. Buhl, C. Reimann, D.A. Pantazis, T. Bredow, F. Neese,
   J. Chem. Theory Comput. 4, 1449 (2008)
- M.M. Quintal, A. Karton, M.A. Iron, A.D. Boese, J.M. Martin, J. Phys. Chem. A 110, 709 (2006)
- C.A. Jiménez-Hoyos, B.G. Janesko, G.E. Scuseria, J. Phys. Chem. A 113, 11742 (2009)
- T. Weymuth, E.P.A. Couzijn, P. Chen, M. Reiher, J. Chem. Theory Comput. 10, 3092 (2014)
- A. Hellweg, C. Hattig, S. Hofener, W. Klopper, Theor. Chem. Acc. 117, 587 (2007)
- 47. F. Neese, J. Am. Chem. Soc. 128, 10213 (2006)
- 48. E.H. Bjarnason, B. Ómarsson, S. Engmann, F.H. Ómarsson, O. Ingólfsson, Eur. Phys. J. D. **68**, 121 (2014)
- R.C. Wetzel, F.A. Baiocchi, T.R. Hayes, R.S. Freund, Phys. Rev. A 35, 559 (1987)
- 50. G.H. Wannier, Phys. Rev. **90**, 817 (1953)
- K.R. Johnson, A.P. Rodriguez, C.R. Brewer, J.A. Brannaka, Z. Shi, J. Yang, B. Salazar, L. McElwee-White, A.V. Walker, J. Chem. Phys. 146, 052816 (2017)
- G. Sbrana, G. Braca, F. Piacenti, P. Pino, J. Organomet. Chem. 13, 240 (1968)
- 53. G.A. Junk, H.J. Svec, Z. Naturforsch. B 23, 1 (1968)
- 54. M.I. Bruce, Adv. Organomet. Chem. 6, 273 (1968)
- 55. R.B. King, J. Am. Chem. Soc. **90**, 1417 (1968)
- O. Ingólfsson, F. Weik, E. Illenberger, Int. J. Mass Spectrom. Ion Processes 155, 1 (1996)
- J. Lengyel, J. Fedor, M. Fárník, J. Phys. Chem. C 120, 17810 (2016)
- M. Zlatar, M. Allan, J. Fedor, J. Phys. Chem. C 120, 10667 (2016)